Nanoscale

MAGNETICALLY ACTUATED LOAD OF FUNCTIONAL RNA NANOPARTICLES

Journal:	*Nanoscale*
Manuscript ID	NR-ART-05-2018-004254.R1
Article Type:	Paper
Date Submitted by the Author:	24-Aug-2018
Complete List of Authors:	Cruz-Acuña, Melissa; University of Florida, J. Crayton Pruitt Family Department of Biomedical Engineering Halman, Justin; University of North Carolina at Charlotte Afonin, Kirill; University of North Carolina at Charlotte, Chemistry Dosbon, Jon; University of Florida, J. Crayton Pruitt Family Department of Biomedical Engineering; University of Florida, Department of Materials Science Rinaldi, Carlos; University of Florida

Nanoscale

ARTICLE

Received 00th May 2018,
Accepted 00th May 20xx
DOI: 10.1039/x0xx00000x
www.rsc.org/

MAGNETICALLY ACTUATED LOAD OF FUNCTIONAL RNA NANOPARTICLES

Melissa Cruz-Acuña,[*a] Justin R. Halman, [b] Kirill A. Afonin, [b] Jon Dobson [a, c] and Carlos Rinaldi [a, d]

RNA is now widely acknowledged not only as a multifunctional biopolymer but also as a dynamic material for constructing nanostructures with various biological functions. Programmable RNA nanoparticles (NPs) allow precise control over their formulation and activation of multiple functionalities, with the potential to self-assemble in biological systems. These attributes make them attractive for drug delivery and therapeutic applications. In the present study, we demonstrate the ability of iron oxide magnetic nanoparticles (MNPs) to deliver different types of RNA NPs functionalized with dicer substrate RNAs inside human cells. Our results show that use of functionalized RNA NPs result in statistically higher transfection efficiency compared to the use of RNA duplexes. Furthermore, we show that the nucleic acids in the MNP/RNA NP complexes are protected from nuclease degradation and that they can achieve knockdown of target protein expression, which is amplified by magnetic stimulus. The current work represents the very first report indicating that iron oxide nanoparticles may efficiently protect and deliver programmable RNA NPs to human cells.

1. Introduction

RNA-based pharmaceuticals hold great promise in the treatment and prevention of chronic and rare diseases such as cancer, diabetes, tuberculosis, and some cardiovascular conditions (1–5). The market for RNA therapeutics appears to dominate over DNA-based therapeutics, with oncology being the leading segment in these efforts (5). These therapeutics take advantage of the RNAi gene regulation process, which occurs after transcription and employs small double-stranded RNAs to direct and prompt homology-dependent gene silencing. The RNAi mechanism is progressively being exploited by using short RNA duplexes, called small-interfering RNAs (siRNAs), for therapeutic gene modulation and treatment of various illnesses (6). More than 20 therapeutic siRNAs are in clinical trials at the moment, and for many establishing an efficient delivery medium is paramount for their success (7).

RNA molecules can be designed to form various stable three-dimensional structures by the use of natural or artificially selected RNA motifs and modules (8–15). The resulting nanoassemblies are fully programmable and their physicochemical and immunological properties can be fine-tuned for particular applications (10,13,16). Nucleic acids, proteins, or small molecules can be individually linked to designed RNA monomers and then brought together with their assemblies (6,13,17). Using rational design, a myriad of structures can be obtained with different connectivity and with precise control over their structure, composition, and modularity. An important aspect of the use of these molecules that has not been fully investigated is the delivery of these RNA NPs inside cells. Their negative charge makes necessary the use of delivery agents that facilitate their endocytosis. Ideally, synthetic agents that facilitate spatial and temporal control over delivery will guarantee appropriate concentration and stoichiometry of therapeutic RNAs locally.

Magnetic nanoparticles (MNPs) coated with positively charged polyethylenimine (PEI) for gene transfection have significantly improved the efficacy of transfection *in vitro*, compared to the use of polycations or lipids alone (18,19). The technique, usually referred to as magnetofection or nanomagnetic transfection, consists of the combination of MNPs with a positively charged coating and nucleic acids to form MNP/NA complexes; addition of these MNP/NA complexes to a culture of adherent cells; and finally placement of a magnet below the cell culture plate. The magnetic field gradient promotes rapid sedimentation of the MNP/NA complex onto the cell surface and enhances endocytosis (20). As a consequence, transfection speed, and for many cell types transfection efficiency, is enhanced compared to no magnetic field exposure or the use of the positively charged coating agent alone. Currently, this technique is being used on a variety of cells and with various designs for the MNPs (21–24). Further, a magnetofection technique using oscillating high-gradient magnetic fields has been reported to cause mechanical stimulation of endocytosis and has resulted in improved transfection efficiency in many cell types compared to the use of static magnets (18).

While much work has been done exploring different aspects of the MNPs used in magnetofection, aside from investigations of incorporation of nuclear location sequences into the transfecting plasmid (25), the design of the nucleic acid cargo has received

[a.] J. Crayton Pruitt Family Department of Biomedical Engineering, University of Florida; 1275 Center Drive, Biomedical Sciences Building JG-56, P.O. Box 116131, Gainesville, Florida, USA, 32611
[b.] Department of Chemistry, University of North Carolina at Charlotte, 9201 University City Blvd, Charlotte, North Carolina, USA, 28223
[c.] Department of Materials Science and Engineering, University of Florida, 549 Gale Lemerand Drive, P.O. Box 116400, Gainesville, Florida, USA, 32611
[d.] Department of Chemical Engineering, University of Florida, 1030 Center Drive, Gainesville, Florida, USA, 32611

comparatively little attention and the use of MNPs to deliver these RNA NPs has not been reported. In the present study, two different RNA NPs, nanorings (26) and nanocubes (27), functionalized with Dicer Substrate (DS) RNAs (28) were combined with PEI-coated MNPs (PEI-MNPs) to form electrostatic interaction-based complexes. RNA NPs chosen for this work exemplify two different design strategies that are currently used in RNA nanotechnology (29). RNA cubes (globular shape) assemble only via the formation of intermolecular canonical Watson-Crick base pairs between the individual monomers designed to avoid any secondary structure formation, while RNA rings (planar) require self-folding of individual RNAs to expose RNA tertiary motifs (kissing loops) that later promote magnesium dependent assembly of cognate monomers. In this study, the ability of the RNA NP/MNP complexes to knockdown EGFP in human breast cancer (MDA-MB-231) cells was evaluated and the knockdown efficiency of each RNA NP/MNP complex was compared. Previous studies that have utilized Lipofectamine 2000 as the transfection agent suggest that functional RNA rings and cubes show high transfection and specific gene (EGFP) silencing efficiencies, while adding multimodal functionalities and increasing resistance to nuclease degradation (6,10,13). In this study, we demonstrate that PEI-MNPs protect nucleic acids against enzymatic degradation as well as an increased efficiency of designed and functionalized RNA structures for protein knockdown, indicative of the efficacy of MNPs for controlled therapeutic delivery.

2. Experimental

Materials

Iron oxide precursor and magnetic nanoparticle synthesis was performed using the following materials: iron acetylacetonate [Fe(acac)3), >98% pure, TCI America; oleic acid (90% technical grade, Sigma-Aldrich); docosane (90% pure, Sigma-Aldrich); 1-octadecene (90% technical grade, SigmaAldrich). The oxygen addition was performed using an air tank containing 20% oxygen and 80% Ar (Airgas), and the argon was added using an argon gas tank from the same company. For MNP aqueous transfer phase and PEI conjugation we used: toluene (certified ACS, Fisher); ethyl acetate (ACS reagent, ≥ 99.5%, Sigma) acetonitrile (anhydrous, ≥ 99.8%, Sigma), sodium periodate (99%, for analysis, ACROS Organics); ethyl alcohol 200 proof from Fisher; branched polyethylenimine with a reported weight-average molecular weight of 25,000 g/mol from Sigma; sulfo-NHS (N-hydroxysulfosuccinimide) and EDC (1-ethyl-3-(3- dimethylaminopropyl)carbodiimidehydrochloride) from ThermoFisher. RNA molecules were synthesized using T7 RNA Polymerase or purchased from Integrated DNA Technologies (IDTDNA.com). All DNA templates and primers (containing T7 promoters) coding for RNA sequences were purchased from IDT. Dithiothreitol (DTT) was purchased from ThermoFisher. The HEPES buffering agent (Fine with crystals/Molecular biology) was purchased from Fisher; while Spermidine (99% GC), Trizma base (99.9% (titration), crystalline), boric acid BioReagent 99.5%, and heparin sodium salt were all purchased from Sigma. We used RQ1 RNase-Free DNase (Promega); urea powder (BioReagent, Sigma) and VWR Life Science Acryl/Bis 37.5:1 when working with native-PAGE to characterize RNA. EGFP-expressing MDA-MB-231 cells were purchased from CellBio Labs; DMEM with 4.5 g/L glucose, fetal bovine serum (USA grade), phosphate buffered saline (sterile), Trypsin-EDTA (0.25%), penicillin at 100 units per mL and streptomycin at 100 mg per mL were purchased from Fisher. RNase ONE™ Ribonuclease was from Promega and Lipofectamine 2000 from ThermoFisher.

Iron Oxide Nanoparticle Synthesis

An iron oleate was prepared following the methods reported by Unni et al., 2017. Briefly, 20.02 g (56.7 mmol) of iron acetylacetonate [Fe(acac)3), >98% pure and 80 g (283.5 mmol) of oleic acid were added to a 500 mL three neck reactor flask. The components were mixed using a Caframo compact overhead stirrer at 350 rpm and 100 sccm of argon. The reaction was heated to about 320 °C at a ramp rate of 8 °C/min. The heating was performed using a fabric heating mantle and temperature controller. A dark brown waxy solid was obtained after 35 minutes at 320 °C. The final product was used as the precursor for the particle synthesis after 24 hours.

To synthesize the iron oxide MNPs, 14.015 g (48.3 mmol) of docosane was heated to 350 °C at a ramp rate of 7−8 °C/min for 50−60 minutes in a 100 mL three-neck reaction flask. Mass flow controllers (Alicat Scientific) regulated the rate of addition of inert gas. Then, 30 mL of iron oleate precursor (0.63 M Fe) mixed with 55 mL of 1-octadecene was added at a controlled rate once the reactor was at 350 °C. An oxygen feed of 20% oxygen and 80% Ar was supplied to the mixture at a rate of 9.47 sccm and controlled using a mass flow controller (Bronkhorst USA). Uniform mixing was done at 350 rpm, and the reaction temperature maintained at 350 °C for 2.5 hours using a temperature controller. Iron oxide nanoparticles were obtained at the end of the reaction after reaction cooled down to room temperature by suspending 5 mL of the black waxy liquid in 10−20 mL of toluene. The particles were purified using 20−40 mL of acetone by centrifuging in an Eppendorf 5430R at 7500 rpm for 10 minutes.

Nanoparticle aqueous phase transfer

The aqueous phase transfer process was performed as previously reported (30) with some modifications. First, 100 mg of dry nanoparticles were suspended in 10 mL of toluene. Then, 10 mL of ethyl acetate/acetonitrile (1:1 by volume) and 8 mL of a 0.28 M sodium periodate ($NaIO_4$) were added. The mixture was ultrasonicated for 20 minutes. Water-soluble particles were magnetically separated and washed with ethanol to remove unreacted reagents. Approximately 80% of the initial MNP mass was recovered and MNPs were then suspended in deionized water. The molar ratio of $NaIO_4$/oleic acid in this procedure was 0.05, based on thermogravimetric analysis on dried MNP and assuming all organic content was oleic acid.

Nanoparticle coating with polyethyleneimine (PEI)

Carbodiimide chemistry was used to conjugate water-soluble MNPs with branched polyethylenimine (31,32). A 10 mg/mL solution of 25 kDa PEI at pH 4.50 – 5 was prepared and placed in an ultrasonicator (Misonix XL2020 Sonicator Ultrasonic Liquid Homogenizer Processor). Then, 10 mg/mL solution of oxidized particles was added slowly, along with 1 mL of water containing sulfo-NHS and EDC at pH 4.5 – 5.0. The mixture was ultrasonicated for an hour. A 450-fold molar excess of amines relative to the estimated carboxylic acid molecules present on the MNP surface was used in this reaction. Estimations were made on the basis of surface area occupied by oleic acid, ~2 oleic acid/nm^2, according to de Palma et al. (33). EDC addition was at 45-fold molar excess to carboxylic acid groups, and a ratio of 1 mole of NHS per 10 moles of EDC was added. Finally, a Millipore filter with a MWCO of 100,000 Da was used to remove unconjugated PEI.

RNA Nanoparticle Synthesis

Each RNA NP is composed of multiple strands programmed to assemble into a larger three-dimensional structure. All DNA templates and primers (containing T7 promoters) coding for RNA sequences were PCR amplified (MyTaq, Bioline), and column purified (Zymo Research). Transcription was accomplished by incubating DNA templates at 37 °C in the presence of home-made T7 RNA polymerase, 100 mM DTT, and transcription buffer (400 mM HEPES-KOH, 10 mM Spermidine, 200 mM DTT, and 120 mM $MgCl_2$). Following incubation for 3.5 hours, the reaction was stopped with RQ1 DNase treatment for 30 minutes, then purified using 8M urea polyacrylamide gel electrophoresis (urea-PAGE, 15% acrylamide) by extracting gel slices and eluting samples into 300 mM NaCl, 1x TBE overnight. The following day, the eluted sample was added to 2x volume of 100% ethanol and cooled at -20 °C for 3 hours. Samples were then spun for 30 minutes at 14000 RCF and the supernatant was disposed. A wash step was performed by adding 90% ethanol and spinning at 14000 RCF for 10 minutes. Finally, the supernatant was disposed, samples were dried using a SpeedVac concentrator, re-suspended in double deionized water, and their concentrations were measured using a NanoDrop2000.

To assemble the RNA NPs, purified single-stranded RNAs were combined in equimolar concentrations in double-deionized water. For rings, the equimolar mixture of all strands was heated to 95 °C for 2 minutes, then snap cooled on ice (4 °C) for 2 minutes. Then, assembly buffer was added (final concentration: 89 mM tris-borate, 50 mM KCl, 2 mM $MgCl_2$) and the samples were incubated at 30 °C for 30 minutes. For cubes, the equimolar solution was heated to 95 °C for 2 minutes, then cooled to 45 °C for thirty minutes. Assembly buffer was added to the cubes after 2 minutes of incubation at 45 °C. Assemblies were confirmed by ethidium bromide total staining non-denaturing native-PAGE (8%, 37.5:1) and atomic force microscopy (AFM).

Atomic force microscopy (AFM)

Freshly cleaved mica was modified with 1-(2-aminopropyl) silatrane according to established protocol. Five microliters of 1 uM RNA samples were deposited onto the modified mica for 2 minutes. Any unbound RNAs and excess salts were washed twice with 50 uL of deionized water and the mica surface was dried with argon gas. AFM imaging was performed on MultiMode AFM Nanoscope IV system (Bruker Instruments, Santa Barbara, CA) in tapping mode. Images were recorded with a 1.5 Hz scanning rate using a TESPA-300 probe from Bruker and a resonance frequency of 320 Hz and spring constant of 40 N/m. Images were processed using FemtoScan Online (Advanced Technologies Center, Moscow, Russia) (34,35).

Dynamic light scattering (DLS) and zeta potential measurements

Dynamic light scattering (Brookhaven Instruments 90Plus/BI-MAS) was used to determine the hydrodynamic size and zeta potential of the MNPs in the various stages of preparation. Nanoparticles coated with PEI were suspended in deionized water. The hydrodynamic diameter distribution was fitted to a lognormal distribution. The zeta potential of the PEI-MNPs was measured in a 10 mM KCl solution at pH 7.

Transmission electron microscopy (TEM)

Particles were imaged using a Hitachi H-7000- Transmission Electron Microscope. Nanoparticles in suspension were deposited on carbon type A copper grids. TEM micrographs were analyzed as described in the protocol available from the National Institute of Standards and Technology (NIST), NCA Joint Assay Protocol PCC-7 (36). The histogram of particle size distribution was fitted to a lognormal size distribution to obtain the number-weighted mean diameter and the geometric deviation of the measurements.

Thermogravimetric analysis (TGA)

The amount of polymer on the particle surface was determined by thermogravimetric analysis (TGA) (TA Instruments Q 6000 STD) in a nitrogen atmosphere. Particles were dried overnight at 80 °C before TGA measurements. The sequence used for the analysis of PEI-MNPs was performed as reported in Cruz-Acuña et al. 2016.

Magnetic Measurements

A Quantum Design superconducting quantum interference device (SQUID) magnetometer (MPMS-3) was used to measure magnetization vs. field. A total of 100 µL of suspended MNP sample were used to perform magnetic measurements at 300 K in a magnetic field range of 7 to -7 T. The experimental saturation magnetization was obtained from the curve by averaging the seven points corresponding to the high-end of the field range. The magnetic diameter of the nanoparticles was calculated by fitting the experimentally determined saturation magnetization to the Langevin model weighted using a lognormal size distribution (37).

RNA binding to PEI-MNPs

RNA binding experiments were carried out on the basis of amine (N) to phosphate (P) ratio (N/P) in the solution being tested. The number of amine nitrogen of the sample (N) was estimated using the polymer content of the sample determined by TGA analysis and assuming all organic content corresponded to PEI (the contribution of azelaic acid was assumed to be negligible). The molecular weights of PEI (25,000 g/mol) and of the repetitive unit (43.07 g/mol) were used to establish the number of N per mole of PEI and the number of moles of amine in the PEI-MNP suspension. The number of phosphates (P) per sample was estimated based on the mass of RNA used, the molecular weight, and the number of base pairs per RNA molecule. With this information we obtained the number of RNA molecules in 0.5 µg and the corresponding number of phosphates per RNA NP.

For the binding experiments, 0.5 µg of RNA NPs in 1x assembly buffer (89 mM tris-borate, 50 mM KCl, 2 mM $MgCl_2$) were mixed with different amounts of PEI-MNPs to achieve various N/P ratios. Each sample was incubated at room temperature for 30 minutes, centrifuged at 7,000 rpm and the RNA content in the supernatant was quantified using a plate reader (Biotek Synergy HT Microplate Reader, using the Take 3 micro-volume plate). Size differences before and after the RNA NP binding were assessed via nanoparticle tracking analysis, using the Nanosight® LM14C.

Nucleic acid protection against nucleases by PEI-MNPs

To assess the ability of the MNPs to protect the nucleic acids from nuclease degradation, DNA duplexes were labeled with Alexa488 (sense 3') and universal quencher Iowa Black (antisense, 5'). When intact, any fluorescence from the Alexa488 was quenched by the Iowa Black; however, when the samples were digested by nuclease activity, the FRET pair leaves its Förster resonance radius, and the Alexa488 fluorescence is detected.

Briefly, DNA duplex with Alexa488 and Iowa black were incubated with MNPs at a 5:1 N:P ratio for 30 minutes at room temperature. Samples were then treated with 3 uL of RQ1 DNase

(Promega) and placed into a Bio-Rad C1000 Touch Thermal Cycler with a CFX96 Real-Time System where the fluorescence was read every thirty seconds. An increase in fluorescence suggests that nuclease activity is able to degrade the nucleic acid sample.

Another experiment was performed to confirm these findings in which PEI-MNPs (1 mg/mL final) were incubated with Alexa488-DNA duplexes (1 µM) for 30 minutes at room temperature. After the complexes had formed, 2 µL of RQ1 DNase and its buffer (40 mM Tris-HCl, 10 mM $MgSO_4$, 1 mM $CaCl_2$) were added and incubated for 30 minutes at 37 °C. To stop the reaction, DNase stop solution (20 mM EGTA) was added and the solution was incubated for 10 minutes at 65 °C according to the manufacturer's protocol. The solution was then centrifuged at 7,500 RCF for 10 minutes and washed with ddH_2O twice. Finally, the solution was resuspended in ddH_2O, and then treated with 0.1 mg/mL heparin sodium salt for 30 minutes at 37 °C. Solutions were then run through a 2% agarose gel.

We also tested nucleic acid protection biologically on MDA-MB-231 EGFP cells. These cells were grown at 37°C and 5% CO_2 in DMEM supplemented with 10% FBS, penicillin at 100 units per mL and streptomycin at 100 mg per mL. Approximately, 10,000 cells per well were seeded on 96-well plate. MNP/Duplex complexes were formed in assembly buffer and RNase ONE™ Ribonuclease from was added. This mixture was incubated for 30 minutes at room temperature, serum-free media was added and mixture was distributed to cells. Cells were exposed to magnetofection using the magnefect-nano™ system with the 96-well plate NdFeB magnet array for 1 hour inside the cell incubator at 37°C. The oscillation amplitude was 200 µm at a frequency of 2.0 Hz. After 1-hour exposure to the magnefect-nanoTM system, the media containing each treatment was removed. Cells were washed with complete media, complete media was added, and knockdown efficiency was evaluated 72 hours after magnetofection via flow cytometry (FACSCanto™ II, BD). This experiment was also performed in serum-containing media. Higher concentration of magnetofectins was required to observe silencing in cells regardless of the presence of RNase (data not shown).

Magnetofection

MDA-MB-231 EGFP cells were grown at 37°C and 5% CO_2 in DMEM supplemented with 10% FBS, penicillin at 100 units per mL and streptomycin at 100 mg per mL. For an initial transfection optimization experiment using duplexes, 10,000 cells were seeded per well in a 96-well plate and incubated for 24 hours. Duplexes were mixed with PEI-MNPs in 100 uL serum free media, incubated for 30 minutes, and more serum free media was added after magnetofectin formation in order for each well to have 100 uL of PEI-MNP/RNA complex-containing media. Magnetofectin solutions were made fresh at different N/P ratios. Media was removed from each well and replaced with media containing magnetofectins. Magnetofection was performed using the magnefect-nano™ system with the 96-well plate NdFeB magnet array for 1 hour inside the cell incubator at 37°C. The oscillation amplitude was 200 µm at a frequency of 2.0 Hz. After 1-hour exposure to the magnefect-nano™ system, the media containing each treatment was removed. Cells were washed with complete media, complete media was added, and knockdown efficiency was evaluated 72 hours after magnetofection via flow cytometry (FACSCanto™ II, BD). GFP expression was measured and optimal N/P ratio was identified. After selecting an efficient N/P ratio, an experiment was performed to compare duplexes, nanorings and nanocubes. The experimental groups were maintained at the same N/P ratio and same amount of duplex addition on all groups was fixed. Therefore, PEI-MNP/Nanorings and PEI-MNP/Nanocubes addition were 6X more concentrated than PEI-MNP/Duplex in terms of PEI-MNP final concentration due to the higher molecular weight and amount of phosphates of cubes and rings. Lipofectamine 2000 and PEI were used as reference and control, respectively; combining it with the same amount of nucleic acid used to form the magnetofectins. Negative controls consisted of cells in complete media and cells exposed to magnetofectins without exposure to the magnetic field. Measurements were taken via flow cytometry (FACSCanto™ II, BD). The same procedure was conducted in the absence of a magnetic field. Viability of cells was measured using CellTiter-Blue® assay 72 hours after treatments using a Biotek Synergy HT.

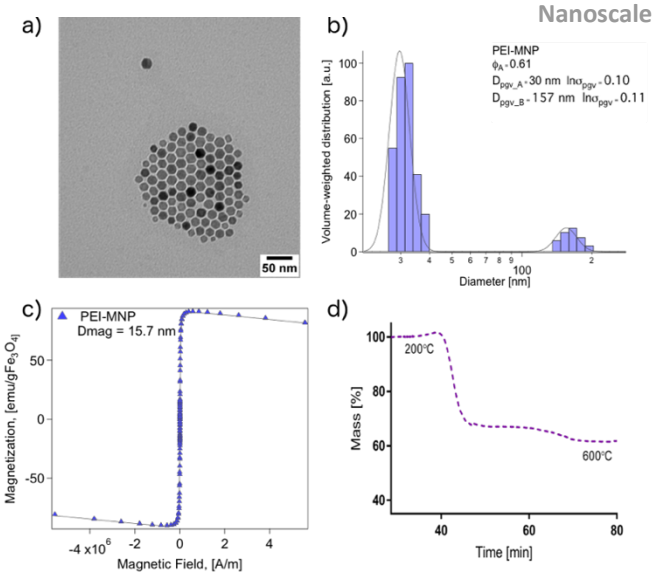

Fig. 1 a) TEM micrograph of as-synthesized MNPs suspended in toluene shows iron oxide nanoparticles of 17 nm (ln σ = 2.89). b) The mean hydrodynamic diameter of the MNPs in water was 30 nm after PEI conjugation (ln σ = 0.10). c) Equilibrium magnetization at 300 K of oleic acid-capped magnetic nanoparticles in suspension shows saturation magnetization value of 80 emu/g of iron oxide and a magnetic diameter of 15.7 nm. d) Thermogravimetric analysis indicates that 61% w/w corresponds to inorganic content on the sample.

PEI-MNPs/RNA Internalization

For the magnetofectin internalization experiment, 10,000 cells per well were seeded in a 96-well plate and incubated for 24 h. Alexa 488 conjugated duplexes, nanorings and nanocubes were used to form magnetofectins at the same N/P ratios used for knockdown experiments. More serum free media was added after RNA binding in order for each well to have 100 uL of PEI-MNP/Alexa488-RNA complex-containing media. Media was removed from each well and replaced with media containing magnetofectins. Magnetofection was performed using the magnefect-nano™ system with the 96-well plate NdFeB magnet array for 1 hour. The oscillation amplitude was 200 µm at a frequency of 2.0 Hz. After 1-hour exposure to the magnefect-nanoTM system, the media containing each treatment was removed. Cells were washed with phosphate buffered saline (PBS). Cells were trypsinized and prepared for flow cytometry analysis. Measurements were taken using the FACSCanto™ II, BD.

The same

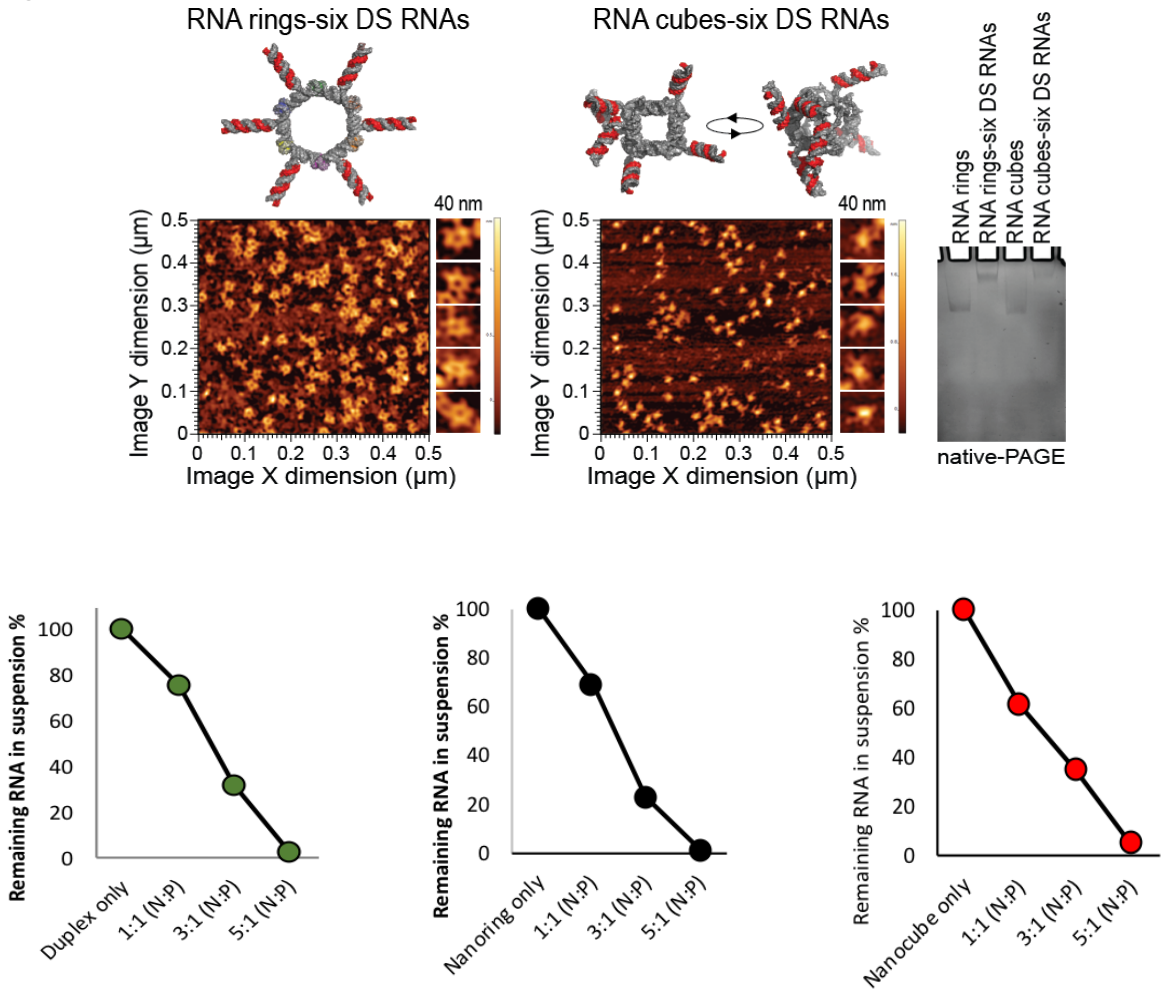

Fig. 2 (Top) Evaluation of nucleic acid nanoparticles via AFM and native-PAGE. Both final RNA rings (top left) and cubes (top middle) are 40 nm in diameter. Change in molecular weight was observed after duplex addition to the structures, which is confirmed on native-PAGE (top right). (Bottom) Evaluation of RNA binding by PEI-MNPs as a function of amine to phosphate ratio (N/P). PEI-MNPs were mixed with RNA Duplexes (bottom left), nanorings (bottom middle), and nanocubes (bottom right) incubated for 30 minutes and centrifuged. The particles efficiently bound to RNA at an N/P of 5:1.

procedure was conducted in the absence of a magnetic field.

3. Results and Discussion

Particle Characterization

Iron oxide nanoparticles were synthesized via the thermal decomposition method, which produced magnetic nanoparticles with a narrow size distribution that are soluble in organic solvent. Aqueous phase transfer was performed, and MNPs were coated with 25kDa branched polyethylenimine via EDC/NHS reaction. Figure 1 shows the results of PEI-MNP physical characterization. The physical size of oleic acid-coated MNPs was measured to be 17 ± 3 nm (Figure 1a). The MNP-PEI volume weighted hydrodynamic diameter was 30 nm, for 60% of the particle volume. The remaining aggregates were particles of ~160 nm (Figure 1b). The saturation magnetization of these PEI-MNPs at 300 K, normalized by iron oxide core mass determined at 300 K, normalized by iron oxide core mass determined from TGA, was 80 emu/g, which is close to bulk value for magnetite (38) and the particles show superparamagnetic behavior. Fitting of the Langevin function weighted by a lognormal size distribution to the equilibrium magnetization curves of Figure 1c yielded a magnetic diameter of 15.7 nm and ln σ = 0.150, which corresponds to an arithmetic diameter of 15.9 nm and a σ = 2.4 nm. TGA measurements showed the organic content of PEI-MNPs was approximately 39 % w/w (Figure 1d). Finally, the measured zeta potential of PEI-MNPs was 34 ± 2.7 mV.

RNA Characterization and Binding Experiments

Functionalized RNA NPs were confirmed by native-PAGE and analyzed using AFM (Figure 2, top). For native-PAGE, non-functionalized RNA NPs were used as controls. The binding of RNA NPs to PEI-MNPs was evaluated as a function of amine to phosphate ratio (N/P) for each of the RNA molecules. Figure 2 (bottom) shows that the relationship between the extent of RNA NP binding and N/P ratios was essentially the same regardless of the type of RNA assembly used. Therefore, it did not appear that ability of PEI-MNPs to bind RNA was affected by the different RNA types and shapes. There was a hydrodynamic size increase after combining PEI-MNPs with the different RNA molecules, shown in Figure 3, which made evident the formation of PEI-MNP/RNA complexes. PEI-MNPs went

from a hydrodynamic diameter of 101 nm (ln σ = 0.750) to 156 nm (ln σ = 0.065) upon binding to RNA duplexes, 165 nm (ln σ = 0.291)

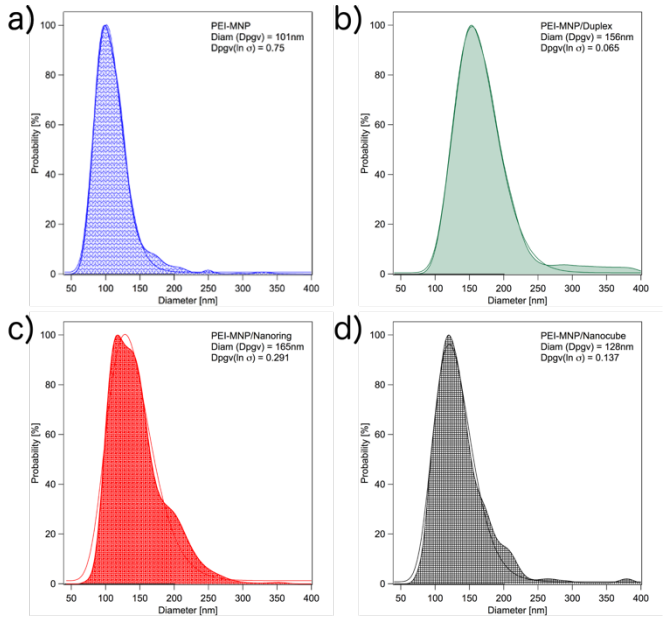

Fig. 3 Nanosight measurements show that PEI-MNPs bind to RNA molecules. PEI-MNPs went from a hydrodynamic diameter of 101 nm (ln σ = 0.750) (a) to 156 nm (ln σ = 0.065) upon binding to RNA duplexes (b), 165 nm (ln σ = 0.291) upon binding to RNA Nanorings (c), and 128 nm (ln σ = 0.750) upon binding to RNA Nanocubes (d).

upon binding to RNA rings, and 128 nm (ln σ = 0.750) upon binding to RNA cubes. We do not expect this size difference between the PEI-MNP/RNA complexes to result in differences in internalization routes in cells.

Nucleic Acid Protection from Nuclease Degradation

To assess the ability of the MNPs to protect the nucleic acids from nuclease degradation, DNA duplexes were labeled with Alexa488 (sense 3') and universal quencher Iowa Black (antisense, 5'). In Figure 4a is shown that when intact, any fluorescence from the Alexa488 was quenched by the Iowa Black; however, when the samples were digested by nuclease activity from DNase, the FRET pair leaves its Förster resonance radius, and the Alexa488 fluorescence is detected. Results show no significant increase in fluorescence of samples incubated with PEI-MNP at N:P of 5:1, which suggests that PEI-MNPs confer protection to the nucleic acid.

Results of additional experiment in agarose gel in Figure 4b show that Alexa488 labelled DNA duplex's size decreases after been exposed to DNase but this size is maintained when DNA duplexes are bound to PEI-MNPs. DNA was detached from PEI-MNPs using heparin and it showed colocalization with not treated DNA sample. Similarly, when testing the integrity of RNA duplexes after their incubation with RNase on EGFP-expressing MDA-MB-231 cells, we observed no EGFP knockdown (Figure 4c). However, when RNA duplexes were complexed with PEI-MNPs, knockdown of EGFP was observed and it was not different from samples containing PEI-MNP/Duplexes in the absence of RNase. Experimental groups in this experiment were all exposed to magnetic field. These results suggest that PEI-MNPs confer protection to the nucleic acid. We believe the PEI coating on the MNPs protects the nucleic acid from RNase and DNase degradations.

Knockdown of EGFP on MDA-MB-231 cells

Knockdown optimizations were performed using different PEI-MNP and RNA duplex amounts within a non-toxic range. Different N/P ratios and PEI-MNP/Duplex concentrations were tested and knockdown efficiency was evaluated 72 hours after EGFP knockdown treatment. After determining the appropriate N/P ratio, the same ratio was used for PEI-MNP/Nanoring and PEI-MNP/Nanocube. In order to be able to compare the efficiency of the different RNA molecules, the concentration of complexes was varied so the total number of duplexes added to each well was 6 times the total moles of RNA nanocubes or nanorings on their corresponding wells. The N/P ratio of the MNP/Duplex found to efficiently knockdown EGFP expression on cells after 1-hour exposure to the magnefect-nano system was 9/1. This high N/P ratio follows previous observations that suggest the complex must be predominantly positively charged to be an effective magnetofection agent (39). Figure 5 summarizes EGFP knockdown outcomes with each letter in the plot indicating statistical difference. When using PEI/RNA complexes and each RNA molecule alone, knockdowns were found to be statistically lower compared to the use of any of the PEI-MNP/RNA complexes in the presence or absence of magnetic field. Under magnetic field stimulation the knockdown efficiency using PEI-MNP/RNAs was

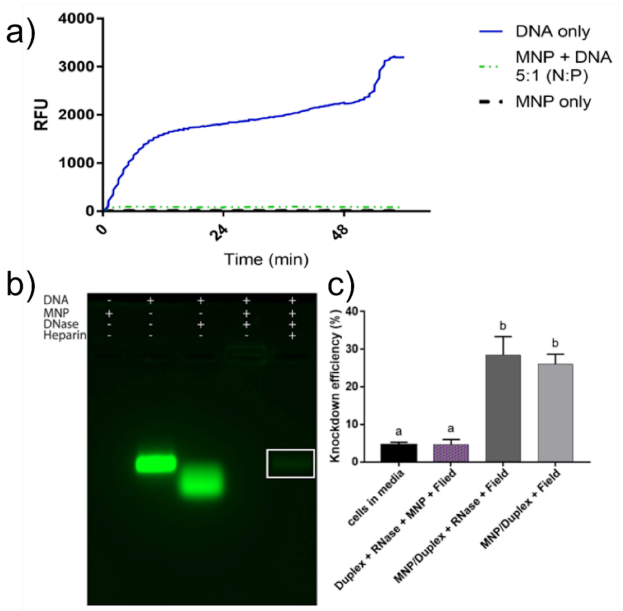

Fig. 4 PEI-MNPs protect RNA molecules from nuclease degradation. (a) The degradation of these complexes was tracked via an increase in fluorescence as the quencher was removed from its fluorophore on DNA duplexes. An increase in fluorescence indicates nuclease activity is able to degrade DNA duplexes, allowing Alexa488 to leave the Forster resonance radius of the quencher Iowa Black. The low fluorescence indicates the efficacy of MNPs to protect DNAs at various concentrations. (b) Degradation of nucleic acid was examined via change in molecular weight on an agarose gel. Alexa488-labelled DNA duplex's size is reduced when exposed to DNase, whereas, nucleic acid from PEI-MNP/Alexa488-labelled DNA duplex maintains its size upon incubation to DNase. This experiment was performed once to confirm the spectroscopic technique results in (a). (c) The ability of RNA in PEI-MNP/Duplex complexes to knockdown EGFP on EGFP-expressing cells is demonstrated and integrity of RNA is confirmed to remain conserved even after incubation of these nanoparticle complexes with RNase. Each letter in the graph indicate statistical difference. We used four replicates per group (n=4) and the experiment was performed once N=1. We performed paired t-tests with 95% confidence interval for statistical analysis. Groups labelled with b have $p < 0.05$ or 0.01 when analyzed against groups labelled with a and have no statistical difference when compared against other b groups. The same occurs with groups labelled with a.

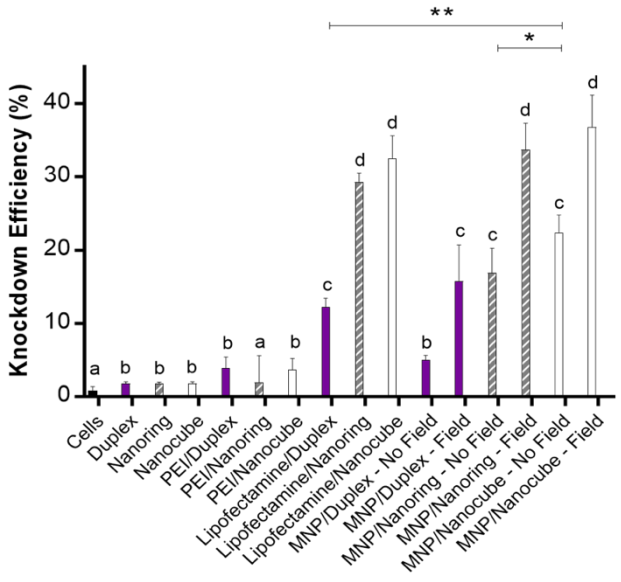

Fig. 5 EGFP knockdown on MDA-MB-231 cells using PEI-MNPs complexed with duplexes, nanorings, and nanocubes, at optimal N/P ratio. Each letter in the graph indicate statistical difference compared to the initial group a (control of cells in media). For example, groups labelled with b have $p < 0.05$ or 0.01 when analyzed against groups labelled with a, c or d and have no statistical difference when compared against other groups labelled with b, unless indicated with asterisks. The same occurs with groups labelled with other letters. Results demonstrated enhanced knockdown efficiency when using PEI-MNPs and magnetic field exposure. This efficiency is similar to their corresponding counterparts when using commercially available Lipofectamine 2000. Nanorings and nanocubes exhibit statistically higher knockdown outcomes when compared to the use of duplexes regardless the type of transfection agent. Four independent experiments were performed and data presented is from one experiment. We performed paired t-tests with 95% confidence interval for statiscial analysis. The number of replicates per group was 4 (n=4). One asterisk (*) indicates $p < 0.05$ and two asterisks (**) indicates $p < 0.01$.

statistically higher than the use of PEI-MNP/RNAs in the absence of magnetic field, PEI/RNA polyplexes, and of the same order as knockdown using the commercial transfection reagent Lipofectamine 2000. Further, EGFP knockdown efficiency results show that RNA nanocubes and RNA nanorings are statistically more efficient at knocking down the expression of EGFP compared to the use of duplexes.

The relatively high knockdown efficiency observed on PEI-MNP/RNA in the presence of magnetic field was attributed to higher levels of PEI-MNP/RNA internalization compared to the groups of PEI-MNP/RNA in the absence of magnetic field. This is shown in Figure 6. In this internalization experiment, results also show that the difference in uptake of PEI-MNPs/Duplexes – magnetic field and without magnetic field is greater compared to the extent of internalization difference observed on the other groups with and without magnetic field. This observation and the fact that PEI-MNPs/RNA complexes are similar in hydrodynamic size distribution suggest that the difference in efficiency between treatment may be due to the RNA structure. The variation in knockdown efficiency observed could be due to the inherent differences within the nucleic acid nanoparticles. Although they are both composed entirely of RNA, they differ in their size, morphology and connectivity. The cubic structures are composed entirely of canonical Watson-Crick base pairing which dictates its structure. The self-assembling strands coalesce to form a three-dimensional globular structure. Highlighting their differences, the nanorings are composed of Watson-Crick base pairing for intra- strand but kissing loop interactions for inter-strand connectivity. The individual monomer strands of the nanorings must form a discrete secondary structure prior to coalescing to form their complete ring. In contrast to the cube, the ring forms a planar two-dimensional construct. The duplexes, for these purposes, may be considered as one-dimensional structures, compared to the nanocubes (3D) and nanorings (2D). The differences in RNAi efficiencies may be attributed to their embedment within the PEI chains. It is possible that the greater knockdown efficiency of the nanorings and nanocubes is due to greater exposure of the nucleic acids to the outside surroundings due to their structure. Therefore, we postulate that it is the PEI-MNP protection of the RNA molecules and the structural differences between nanorings and nanocubes promotes stability in the cell environment, which allows for enhanced EGFP knockdown. In addition, another advantage of the use PEI-MNP/RNA complexes lies in the ability to control when and where knockdown is promoted through the application of the magnetic field stimulus, which results in knockdown upon only 1 hour of magnetofection treatment if desired.

Finally, viability was evaluated after EGFP knockdown to assess if the presence of the RNA, knockdown of the EGFP, or uptake promoted by magnetic stimulation had any effect on cells. The results are summarized in Fig. 7. Neither the PEI-MNPs nor the control and reference groups tested were found toxic to MDA-MB-231 cells 72 hours after knockdown treatments.

4. Conclusions

We report the use of PEI-coated iron oxide magnetic nanoparticles as a delivery agent of complex RNA NPs into cells. In this study, we tested EGFP knockdown using synthetic RNA NPs of different designs. We demonstrated that PEI-MNPs enhance knockdown outcome due to an increase in magnetofectin internalization promoted by an oscillating magnetic field gradient while at the same time protecting the nucleic acid from degradation. Duplexes, nanorings, and nanocubes (the latter two containing 6 duplexes each) were used to study how EGFP knockdown outcome was affected by the RNA molecule structural design. Nanorings and nanocubes demonstrated that structural characteristics of RNA molecules provide enhanced knockdown efficiency. The use of functional RNA molecules guarantees a higher concentration and desired stoichiometry of therapeutic moieties locally. This technology in combination with MNPs is a powerful tool for spatial and temporal therapeutic delivery control.

Conflicts of interest

There are no conflicts to declare.

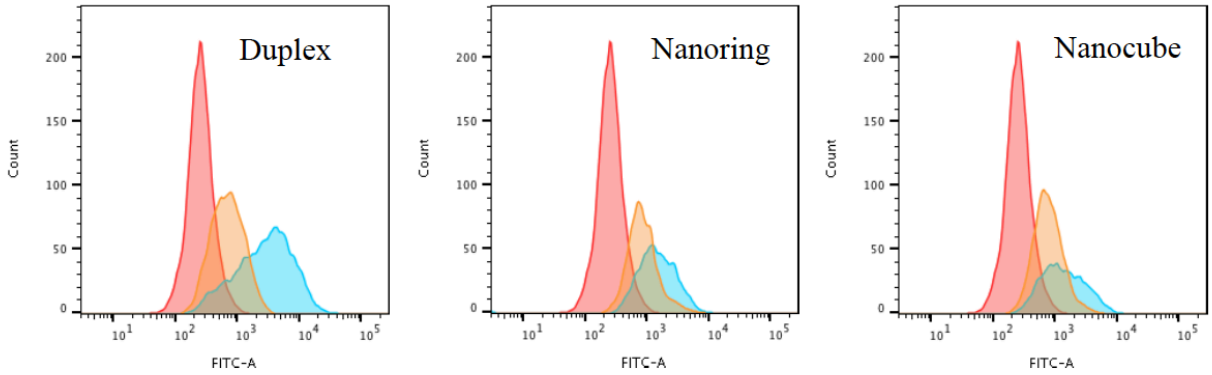

Fig. 6 PEI-MNP/Nucleic acid complex internalization is enhanced when using magnetic field gradient. Alexa488 conjugated to complementary DNA structures of each RNA molecule of the study were used to asses PEI-MNP/Nucleic acid internalization of duplexes, nanorings, and nanocubes. In all cases of cells exposed to PEI-MNP/RNA complexes in the presence of magnetic field (blue), the internalization of complexes was greater than in the absence of the magnetic field (orange). Internalization of complexes was still observed in the absence of the magnetic field when compared to cell control (red). This experiment was performed twice with three replicates per experimental group and control (n=3). Data shown is one representative n (or well) per experimental group and control.

Acknowledgements

The research was supported by Department of Chemistry UNC Charlotte start-up funds to KA. Authors would like to thank Dr. Alexander Lushnikov and Dr. Alexey Krasnoslobodtsev for performing AFM imaging of the nanoparticles at the Nanoimaging core facility at the University of Nebraska Medical Center. We also want to thank graduate student Shehaab Savliwala for the TEM micrographs. At UF, this work was sponsored in part by the National Science Foundation (HRD-1345156).

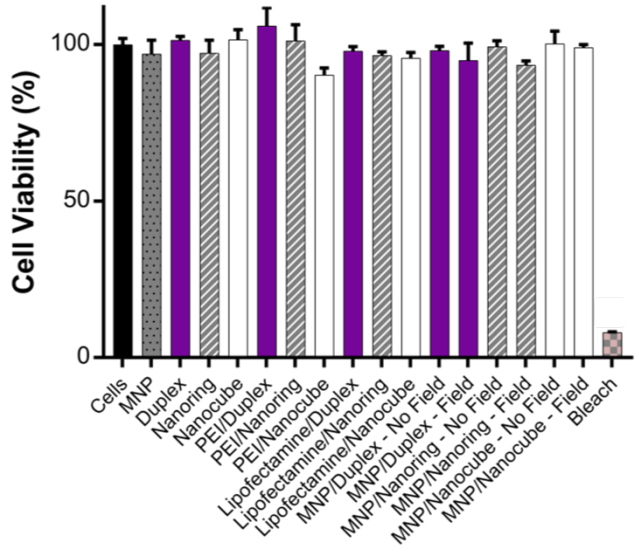

Fig. 7 Viability of MDA-MB-231 cells exposed to PEI-MNP complexed with duplexes, nanorings, or nanocubes evaluated 72 hours after 1-hour exposure to oscillating magnetic field.). None of the groups obtained a mean viability below 80% except for the positive control treated with 10% bleach (Bleach).. Cell viability was obtained by running CellTiter-Blue® assay. Assay was performed 72 hours post transfection. Mean fluorescent units obtained for each treatment were normalized with mean fluorescence obtained from cells in complete media (Cells). Four wells per group were analyzed (n =4).

References

1. Ying H, Zaks TZ, Wang RF, Irvine KR, Kammula US, Marincola FM, et al. Cancer therapy using a self-replicating RNA vaccine. Nat Med [Internet]. 1999;5(7):823–7. Available from: http://dx.doi.org/10.1038/10548
2. Sapir T, Shternhall K, Meivar-Levy I, Blumenfeld T, Cohen H, Skutelsky E, et al. Cell-replacement therapy for diabetes: Generating functional insulin-producing tissue from adult human liver cells. Proc Natl Acad Sci U S A. 2005;102(22):7964–9.
3. Wang P, Yigit M V., Medarova Z, Wei L, Dai G, Schuetz C, et al. Combined small interfering RNA therapy and in vivo magnetic resonance imaging in islet transplantation. Diabetes. 2011;60(2):565–71.
4. Lorenzi JCC, Trombone APF, Rocha CD, Almeida LP, Lousada RL, Malardo T, et al. Intranasal vaccination with messenger RNA as a new approach in gene therapy: Use against tuberculosis. BMC Biotechnol [Internet]. 2010;10:1–11. Available from: http://www.embase.com/search/results?subaction=viewrecord&from=export&id=L51121170%5Cnhttp://www.biomedcentral.com/1472-6750/10/77%5Cnhttp://dx.doi.org/10.1186/1472-6750-10-77%5Cnhttp://sfx.library.uu.nl/utrecht?sid=EMBASE&issn=14726750&id=doi:10.1186/147
5. Pai SI, Lin Y-Y, Macaes B, Meneshian A, Hung C-F, Wu T-C. Prospects of RNA interference therapy for cancer. Gene Ther [Internet]. 2006;13(6):464–77. Available from: http://www.nature.com/doifinder/10.1038/sj.gt.330

2694
6. Afonin KA, Viard M, Koyfman AY, Martins AN, Kasprzak WK, Panigaj M, et al. Multifunctional RNA nanoparticles. Nano Lett. 2014;14(10):5662–71.
7. Kaczmarek JC, Kowalski PS, Anderson DG. Advances in the delivery of RNA therapeutics: from concept to clinical reality. Genome Med [Internet]. Genome Medicine; 2017;9(1):60. Available from: http://genomemedicine.biomedcentral.com/articles/10.1186/s13073-017-0450-0
8. Jasinski D, Haque F, Binzel DW, Guo P. Advancement of the Emerging Field of RNA Nanotechnology. ACS Nano. 2017;11(2):1142–64.
9. Shukla GC, Haque F, Tor Y, Wilhelmsson LM, Toulmé JJ, Isambert H, et al. A boost for the emerging field of RNA nanotechnology report on the First International Conference on RNA nanotechnology. ACS Nano. 2011;5(5):3405–18.
10. Halman JR, Satterwhite E, Roark B, Chandler M, Viard M, Ivanina A, et al. Functionally-interdependent shape-switching nanoparticles with controllable properties. Nucleic Acids Res. 2017;45(4):2210–20.
11. Afonin KA, Kasprzak WK, Bindewald E, Kireeva M, Viard M, Kashlev M, et al. In silico design and enzymatic synthesis of functional RNA nanoparticles. Acc Chem Res. 2014;47(6):1731–41.
12. Afonin KA, Kireeva M, Grabow WW, Kashlev M, Jaeger L, Shapiro BA. Co-transcriptional assembly of chemically modified RNA nanoparticles functionalized with siRNAs. Nano Lett. 2012;12(10):5192–5.
13. Afonin KA, Viard M, Kagiampakis I, Case CL, Dobrovolskaia MA, Hofmann J, et al. Triggering of RNA Interference with RNA-RNA, RNA-DNA, and DNA-RNA Nanoparticles. 2015;251–9.
14. Afonin KA, Viard M, Tedbury P, Bindewald E, Parlea L, Howington M, et al. The Use of Minimal RNA Toeholds to Trigger the Activation of Multiple Functionalities. Nano Lett. 2016;16(3):1746–53.
15. Grabow WW, Jaeger L. RNA self-assembly and RNA nanotechnology. Acc Chem Res. 2014;47(6):1871–80.
16. Johnson MB, Halman JR, Satterwhite E, Zakharov A V., Bui MN, Benkato K, et al. Programmable Nucleic Acid Based Polygons with Controlled Neuroimmunomodulatory Properties for Predictive QSAR Modeling. Small. 2017;13(42).
17. Afonin KA, Viard M, Martins AN, Lockett SJ, Maciag AE, Freed EO, et al. Activation of different split functionalities on re-association of RNA–DNA hybrids. Nat Nanotechnol [Internet]. Nature Publishing Group; 2013;8(4):296–304. Available from: http://www.nature.com/doifinder/10.1038/nnano.2013.44
18. McBain SC, Griesenbach U, Xenariou S, Keramane a, Batich CD, Alton EWFW, et al. Magnetic nanoparticles as gene delivery agents: enhanced transfection in the presence of oscillating magnet arrays. Nanotechnology. 2008;19(40):405102.
19. Kamau SW, Hassa PO, Steitz B, Petri-Fink A, Hofmann H, Hofmann-Amtenbrink M, et al. Enhancement of the efficiency of non-viral gene delivery by application of pulsed magnetic field. Nucleic Acids Res. 2006;34(5):1–8.
20. Schillinger U, Brill T, Rudolph C, Huth S, Gersting S, Krötz F, et al. Advances in magnetofection—magnetically guided nucleic acid delivery. J Magn Magn Mater [Internet]. 2005 May [cited 2014 Jul 19];293(1):501–8. Available from: http://linkinghub.elsevier.com/retrieve/pii/S0304885305001216
21. Scherer F, Anton M, Schillinger U, Henke J, Bergemann C, Krüger A, et al. Magnetofection-enhancing and targeting gene delivery by magnetic force in vitro and in vivo.pdf. Gene Ther. 2002;9:102–9.
22. Tang Y-S, Wang D, Zhou C, Ma W, Zhang Y-Q, Liu B, et al. Bacterial magnetic particles as a novel and efficient gene vaccine delivery system. Gene Ther. 2011;5(May 2011):1187–95.
23. Cheong SJ, Lee CM, Kim SL, Jeong HJ, Kim EM, Park EH, et al. Superparamagnetic iron oxide nanoparticles-loaded chitosan-linoleic acid nanoparticles as an effective hepatocyte-targeted gene delivery system. Int J Pharm. 2009;372(1–2):169–76.
24. Leder A, Raschzok N, Schmidt C, Arabacioglu D, Butter A, Kolano S, et al. Micron-sized iron oxide-containing particles for microRNA-targeted manipulation and MRI-based tracking of transplanted cells. Biomaterials [Internet]. Elsevier Ltd; 2015;51:129–37. Available from: http://dx.doi.org/10.1016/j.biomaterials.2015.01.065
25. Vernon MM, Dean DA, Dobson J. DNA targeting sequence improves magnetic nanoparticle-based plasmid DNA transfection efficiency in model neurons. Int J Mol Sci. 2015;16(8):19369–86.
26. Grabow WW, Zakrevsky P, Afonin KA, Chworos A, Shapiro BA, Jaeger L. Self-assembling RNA nanorings based on RNAI/II inverse kissing complexes. Nano Lett. 2011;
27. Afonin KA, Bindewald E, Yaghoubian AJ, Voss N, Jacovetty E, Shapiro BA, et al. In vitro assembly of cubic RNA-based scaffolds designed in silico. Nat Nanotechnol. 2010;5(9):676–82.
28. Rose SD, Kim DH, Amarzguioui M, Heidel JD, Collingwood MA, Davis ME, et al. Functional polarity is introduced by Dicer processing of short substrate RNAs. Nucleic Acids Res. 2005;33(13):4140–56.
29. Afonin KA, Grabow WW, Walker FM, Bindewald E, Dobrovolskaia MA, Shapiro BA, et al. Design and self-

assembly of siRNA-functionalized RNA nanoparticles for use in automated nanomedicine. Nat Protoc. 2011;6(12):2022–34.

30. Cruz-Acuña M, Maldonado-Camargo L, Dobson J, Rinaldi C. From oleic acid-capped iron oxide nanoparticles to polyethyleneimine-coated single-particle magnetofectins. J Nanoparticle Res. 2016;18(9).
31. Kasturi SP, Sachaphibulkij K, Roy K. Covalent conjugation of polyethyleneimine on biodegradable microparticles for delivery of plasmid DNA vaccines. Biomaterials. 2005;26(32):6375–85.
32. Kim H, Namgung R, Singha K, Oh IK, Kim WJ. Graphene oxide-polyethylenimine nanoconstruct as a gene delivery vector and bioimaging tool. Bioconjug Chem. 2011;22(12):2558–67.
33. De Palma R, Peeters S, Van Bael MJ, Van Den Rul H, Bonroy K, Laureyn W, et al. Silane ligand exchange to make hydrophobic superparamagnetic nanoparticles water-dispersible. Chem Mater. 2007;19(7):1821–31.
34. Shlyakhtenko LS, Gall AA, Filonov A, Cerovac Z, Lushnikov A, Lyubchenko YL. Silatrane-based surface chemistry for immobilization of DNA, protein-DNA complexes and other biological materials. Ultramicroscopy. 2003;
35. Luda S, Alexander AG, Yuri L. Mica functionalization for imaging of dna and protein-dna complexes with atomic force microscopy. Methods Mol Biol. 2012;
36. Bonevich J, Haller W. Measuring the Size of Nanoparticles Using Transmission Electron Microscopy (TEM). NIST-NCL Jt Assay Protoc PCC-7. 2010;21702(February):1–13.
37. Neuringer JL, Rosensweig RE. Ferrohydrodynamics. Phys Fluids [Internet]. 1964;7(12):1927–37. Available from: http://www.scopus.com/inward/record.url?eid=2-s2.0-0041140815&partnerID=tZOtx3y1
38. Khandhar AP, Ferguson RM, Krishnan KM. Monodispersed magnetite nanoparticles optimized for magnetic fluid hyperthermia: Implications in biological systems. J Appl Phys. 2011;109(7):10–3.
39. Boussif O, Lezoualc'h F, Zanta MAntoniet, Mergny MD, Scherman D, Demeneix B, et al. A versatile vector for gene and oligonucleotide transfer into cells in culture and in vivo: polyethylenimine. Proc Natl Acad Sci U S A [Internet]. 1995;92(16):7297–301. Available from: http://www.pubmedcentral.nih.gov/articlerender.fcgi?artid=41326&tool=pmcentrez&rendertype=abstract

